

Physical, Thermal, and Spectroscopic Characterization of Biofield Energy Treated Methyl-2-Naphthyl Ether

Mahendra Kumar Trivedi¹, Alice Branton¹, Dahryn Trivedi¹, Gopal Nayak¹, Khemraj Bairwa² and Snehasis Jana^{2*}

¹Trivedi Global Inc., 10624 S Eastern Avenue Suite A-969, Henderson, NV 89052, USA

²Trivedi Science Research Laboratory Pvt. Ltd., Hall-A, Chinar Mega Mall, Chinar Fortune City, Hoshangabad Rd., Bhopal- 462026, Madhya Pradesh, India

Abstract

Methyl-2-naphthyl ether (MNE) is an organic compound and used as the primary moiety for the synthesis of several antimicrobial and anti-inflammatory agents. This study was attempted to evaluate the impact of biofield energy treatment on the physical, thermal, and spectroscopic properties of MNE. The study was carried out in two groups i.e., control and treated. The treated group was subjected to Mr. Trivedi's biofield treatment. Afterward, the control and treated samples of MNE were evaluated using X-ray diffraction (XRD), surface area analyzer, differential scanning calorimetry (DSC), thermogravimetric analysis-derivative thermogravimetric analysis (TGA-DTG), Fourier transform infrared (FT-IR), and ultraviolet-visible (UV-Vis) spectroscopy. The XRD study exhibited the decrease in average crystallite size by 30.70%. The surface area analysis showed 5.32% decrease in surface area of the treated sample with respect to the control. The DSC thermogram of treated MNE exhibited no significant change in the melting temperature; however, the latent heat of fusion was slightly increased (0.83%) after biofield treatment as compared to the control sample. The TGA analysis showed the onset temperature of thermal degradation at 158°C in the control sample that was reduced to 124°C after biofield treatment. The result showed about 21.52% decrease in onset temperature of thermal degradation of treated MNE as compared to the control. Similarly, the end-set temperature of thermal degradation was also reduced by 13.51% after biofield treatment with respect to the control. The FT-IR and UV spectroscopic studies did not show any changes in the wavenumber and wavelength, respectively in treated MNE with respect to the control. Overall, the XRD, surface area and thermal analysis suggest that biofield treatment has the impact on physical and thermal properties of the treated MNE as compared to the control.

Keywords: Methyl-2-naphthyl ether; Biofield energy; X-ray diffraction; Surface area analysis; Differential scanning calorimetry; Thermogravimetric analysis

Abbreviations

MNE: Methyl-2-Naphthyl Ether; NCCAM: National Center For Complementary And Alternative Medicine; XRD: X-Ray Diffraction; DSC: Differential Scanning Calorimetry; TGA: Thermogravimetric Analysis; DTA: Differential Thermal Analysis; DTG: Derivative Thermogravimetry; FT-IR: Fourier Transforms Infrared

Introduction

Naphthalene has been described as new class of potent antimicrobials against wide range of human pathogens. It occupies a central place among biologically active compounds owing to its varied and exciting antibiotic properties with less toxicity [1]. Numerous naphthalene containing antimicrobial drugs are existing like naftifine, nafcillin, terbinafine, tolnaftate, etc. that plays vital role against microbial infections [2,3]. Further, the naphthalene derivatives like naproxen, nabumetone were also studied in depth as the nonsteroidal anti-inflammatory drugs (NSAIDs). They are mainly nonselective inhibitor of two cyclooxygenase (COX) isoform i.e., COX-1 and COX-2 [4,5]. Moreover, the structurally relative naphthalene derivatives lower the parathyroid level by binding to calcium receptor on the parathyroid gland. Thus, it helps to regulate hyperparathyroidism especially in kidney disease or parathyroid gland neoplasm [6]. Based on the importance of naphthalene derivative as a main moiety for organic synthesis of several pharmaceutical drugs, it is advantageous to find out the alternate approach that can enhance the physicochemical and thermal properties of naphthalene derivative i.e., methyl-2-naphthyl ether (MNE). Recently, an alternate treatment approach i.e., healing therapy or therapeutic touch, known as the biofield energy treatment, which was reported in several fields. The National Institute of Health/National Center for Complementary and Alternative Medicine (NIH/NCCAM) conceived the biofield energy treatment in subcategory of energy therapies (putative energy fields) [7,8]. The biofield treatment is

being used in healing process to reduce pain, anxiety and to promote the overall health of human being [9,10]. Biofield is an electromagnetic field that permeates and surrounds living organisms. This biologically produced electromagnetic and subtle energy field regulates the various physiological and communications functions within the human organism [11]. Researchers have attempted different biological studies and effects of biofield on various biomolecules such as proteins, antibiotics [12], bacterial cultures [13], and conformational change in DNA [14]. Prakash et al. reported that various scientific instruments such as Kirlian photography, resonance field imaging (RFI) and polycontrast interference photography (PIP) could be extensively used to measure the biofield of human body [15]. Thus, the human has the ability to harness the energy from the environment or Universe and transmit it to any living or nonliving object on the Globe. The object(s) receive the energy and respond into the useful way; this process is termed as biofield treatment. Mr. Trivedi's unique biofield energy treatment is known as 'The Trivedi Effect'. Recently, biofield energy treatment has been described as an alternative method to alter the physicochemical and thermal properties of several metals and ceramics [16-18]. It has also reported to alter the spectroscopic properties of various pharmaceutical drugs like paracetamol, piroxicam, metronidazole, and tinidazole [19,20]. Moreover, the biofield treatment has been studied in

***Corresponding author:** Snehasis Jana, Trivedi Science Research Laboratory Pvt. Ltd., Hall-A, Chinar Mega Mall, Chinar Fortune City, Hoshangabad Rd., Bhopal-462026 Madhya Pradesh, India, Tel: 91-755-6660006; E-mail: publication@trivedisrl.com

Received September 07, 2015; **Accepted** September 14, 2015; **Published** September 20, 2015

Citation: Trivedi MK, Branton A, Trivedi D, Nayak G, Bairwa K, et al. (2015) Physical, Thermal, and Spectroscopic Characterization of Biofield Energy Treated Methyl-2-Naphthyl Ether. J Environ Anal Chem 2: 162. doi:10.4172/2380-2391.1000162

Copyright: © 2015 Trivedi MK, et al. This is an open-access article distributed under the terms of the Creative Commons Attribution License, which permits unrestricted use, distribution, and reproduction in any medium, provided the original author and source are credited.

several fields like agriculture research [21,22], biotechnology research [23], and microbiology research [24,25].

Based on the published literature and outstanding impact of biofield energy treatment on various living and nonliving things, the present study was aimed to evaluate the impact of Mr. Trivedi's biofield energy treatment on physical, thermal and spectroscopic properties of MNE using several analytical techniques.

Materials and Methods

Study design

The Methyl-2-Naphthyl Ether was procured from Sisco Research Laboratories, India. The study was performed in two groups i.e., control and treated. The control sample was remained as untreated, and the treated group in sealed pack was handed over to Mr. Trivedi for biofield energy treatment under laboratory conditions. Mr. Trivedi provided the biofield energy treatment to the treated group through his unique energy transmission process without touching the sample. Subsequently, the control and treated samples of MNE were analyzed using several analytical techniques like X-ray diffraction (XRD), surface area analysis, differential scanning calorimetry (DSC), thermogravimetric analysis (TGA), Fourier transform infrared (FT-IR), and ultraviolet-visible (UV-Vis) spectroscopy.

XRD study

The XRD analysis of the control and treated MNE was carried out on Phillips, Holland PW 1710 X-ray diffractometer with nickel filter and copper anode. The wavelength used in XRD system was 1.54056 Å. The XRD diffractograms were obtained in the form of a chart of 2θ vs. intensity. The crystallite size (G) and percent change in crystallite size of MNE were calculated using the following equations [26].

$$\text{Crystallite size (G)} = k\lambda / (b \cos\theta)$$

$$\text{Percent change in crystallite size (G)} = [(G_t - G_c) / G_c] \times 100$$

Where, G_c and G_t are average crystallite size of control and treated powder samples respectively.

Surface area analysis

The surface area of the control and treated MNE was measured using the Brunauer–Emmett–Teller (BET) surface area analyzer, Smart SORB 90. Percent change in surface area was calculated using following equation:

$$\% \text{ change in surface area} = \frac{[S_{\text{Treated}} - S_{\text{Control}}]}{S_{\text{Control}}} \times 100$$

Where, S_{Control} and S_{Treated} are the surface area of the control and treated samples, respectively.

DSC study

The control and treated samples of MNE were studied using a Pyris-6 Perkin Elmer differential scanning calorimeter on a heating rate of 10°C/min under air atmosphere with air flow rate of 5 mL/min. An empty pan sealed with cover was used as a reference pan. The melting temperature (T_m) and latent heat of fusion (ΔH) were obtained from the DSC curve.

TGA-DTG analysis

TGA-DTG analysis was conducted to investigate the thermal stability of the control and treated MNE. The studies were carried out on Mettler Toledo simultaneous TGA-DTG system. Both the control and treated samples were heated from room temperature to 400°C with

a heating rate of 5°C/min under air atmosphere. The onset temperature of thermal degradation and percent change in temperature at which maximum weight loss occur in samples were obtained from DTG thermogram.

Spectroscopic studies

For the purpose of FT-IR and UV-Vis spectroscopic characterization, the treated sample was divided into two groups i.e., T1 and T2. Both the treated groups were then analyzed for spectroscopic characteristics employing FT-IR and UV-Vis spectroscopy and data were compared with the respective spectrum of control sample.

FT-IR spectroscopic characterization

The samples for FT-IR spectroscopy were prepared by crushing into fine powder and then mixing in spectroscopic grade KBr. Finally, the mixture was pressed into pellets with a hydraulic press and then used for analysis. The spectra were recorded from Shimadzu's Fourier transform infrared spectrometer (Japan) with the frequency range of 4000-500 cm^{-1} . The analysis was done to evaluate the impact of biofield energy treatment at the atomic levels like force constant, dipole moment, and bond strength in chemical structure [27].

Uv-Vis spectroscopic analysis

The samples solutions for UV spectroscopy were prepared in methanol. UV spectra of the control and treated samples of MNE were acquired from Shimadzu UV-2400 PC series spectrophotometer with quartz cuvette having slit widths of 2.0 nm. The wavelength was set between 200-400 nm for analysis. The study was carried out to evaluate the impact of biofield energy treatment on the energy gap of highest occupied molecular orbital and lowest unoccupied molecular orbital (HOMO–LUMO gap) [27].

Results and Discussion

XRD analysis

XRD diffractograms of both control and treated MNE are shown in Figure 1. The control sample exhibited the XRD peaks at 2θ equal to 10.27°, 15.44°, 19.07°, 20.57°, 21.21°, 24.76°, 25.33°, and 28.77°. Likewise, the XRD diffractogram of treated MNE showed the XRD peaks at 2θ equal to 10.25°, 15.30°, 19.01°, 20.55°, 21.17°, 24.67°, 25.25°, and 28.84°. The intensity of peak was also altered after biofield energy treatment as compared to the control. XRD diffractograms of both the control and treated MNE showed the intense peaks, which suggest the crystalline nature of MNE. The decrease of XRD peaks intensity in treated sample might be attributed to the reduction in crystallinity and decrease in long-range order of the molecules. The crystallite size was calculated using Scherrer formula and the results are shown in Figure 2. The average crystallite size of the control MNE was observed as 84.55 nm that was decreased up to 58.59 nm in the treated sample. The result indicated about 30.70% decrease in average crystallite size of treated sample with respect to the control.

The increase in internal micro strain leads to decrease the corresponding crystallite size of the material [28]. Moreover, Zhang *et al.* reported that presence of strain and increased atomic displacement from their ideal lattice positions lead to reduction in crystallite size [29]. Hence, it is assumed that biofield energy treatment probably induce the internal strain in treated MNE sample. This might be responsible for the decrease in crystallite size of the treated MNE as compared to the control.

Surface area analysis

The surface area of control and treated samples of MNE were

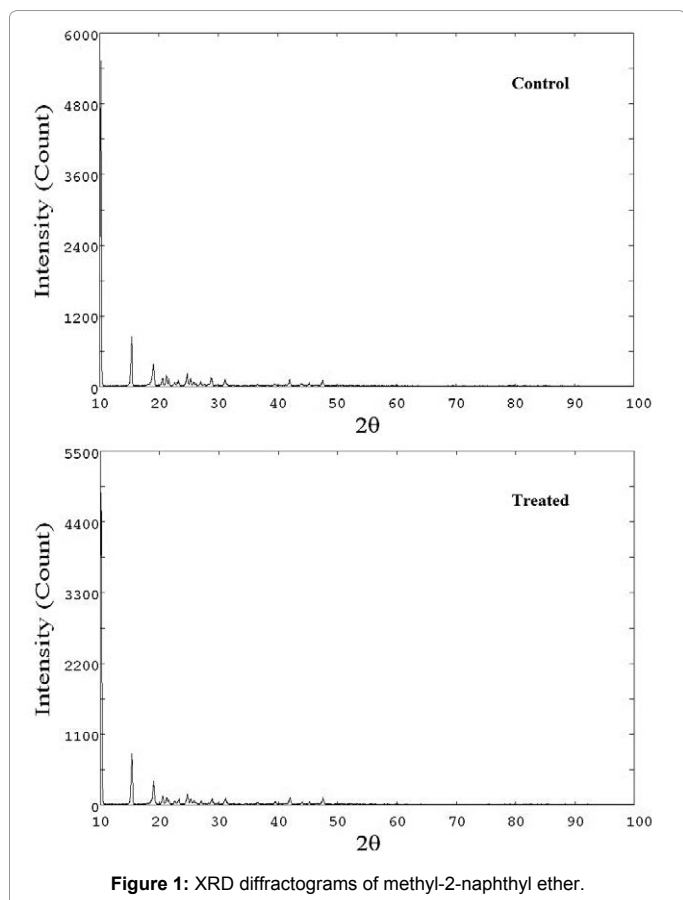


Figure 1: XRD diffractograms of methyl-2-naphthyl ether.

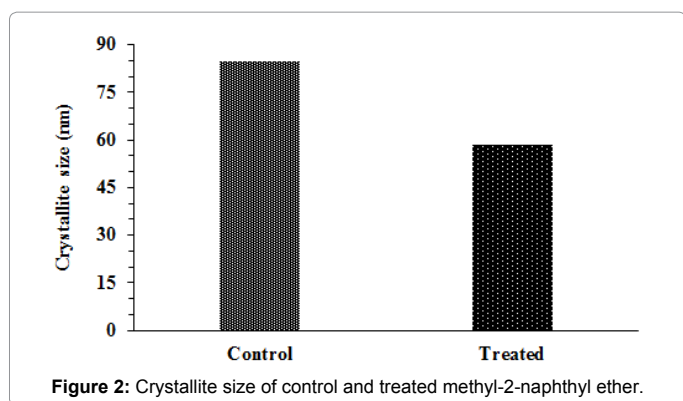


Figure 2: Crystallite size of control and treated methyl-2-naphthyl ether.

determined using BET surface area analyzer and data are presented in Figure 3. The surface area of the control and treated sample was observed as 0.4904 m²/g and 0.4643 m²/g, respectively. The result showed a considerable decrease in surface area i.e., 5.32% in the treated MNE as compared to the control sample. It is assumed that biofield energy treatment possibly induced the disappearance of inter-particle boundaries that may lead to the aggregation of particles and thus increase in particle size [30]. Presumably, this increase in particle size might lead to decrease in surface area of the treated sample.

DSC analysis

DSC analysis was performed to determine the melting temperature and latent heat of fusion (ΔH) of the control and treated MNE. DSC thermograms (Figure 4) of MNE showed the melting temperature at 73.72°C in the control and 73.66°C in the treated sample (Table 1). The

result depicted no significant change in melting temperature of treated sample as compared to the control. The melting temperature of control MNE was well supported by literature data [31]. DSC thermogram exhibited the ΔH of 147.49 J/g in control sample and 148.72 J/g in treated sample of MNE. The result showed about 0.83% increase in latent heat of fusion of treated sample as compared to the control. It is hypothesized that biofield energy treatment may cause absorption of energy during the phase transition from solid to liquid that might lead to increase the latent heat of fusion of treated sample with respect to the control. Previously, our group has reported that biofield energy treatment altered the value of latent heat of fusion in lead and tin powders [7].

TGA-DTG analysis

The TGA and DTG thermograms of control and treated samples of MNE are shown in Figure 5 and data are reported in Table 1. The onset temperature of thermal degradation was observed at 158°C and 124°C for the control and treated samples, respectively. Whereas, the end-set temperature of thermal degradation was found at 201°C and 178°C in the control and treated sample, respectively. The result showed about 21.52% decrease in the onset temperature and 11.44% decrease in the end-set temperature in treated sample with respect to the control. The percent weight loss during thermal decomposition was 63.41% in the control and 59.18% in the treated sample. It showed the decrease in % weight loss during thermal decomposition after biofield treatment. Based on this, it is presumed that biofield treated MNE may be more stable as compared to the control. The DTG thermogram exhibited the T_{max} (the temperature at which the sample lost its maximum weight) at 177.81°C in the control sample and at 153.78°C in the treated sample of MNE. The result revealed about 13.51% decrease in T_{max} of treated sample with respect to the control. This decrease in T_{max} in treated sample might be due to increase in vaporization or volatilization [32] of treated MNE molecules after biofield energy treatment. It might be correlated with the alteration in internal energy through biofield energy treatment that results into earlier vaporization in treated sample as compared to the control.

FT-IR spectroscopic analysis

FT-IR spectra of the control and treated samples of MNE (Figure 6) were inferred using the theoretically predicted wavenumber. The aromatic =C-H stretching peak was assigned at 3007-3057 cm⁻¹ in all three samples i.e., the control and treated (T1 and T2). Likewise, the -C-H (methyl) stretching was attributed to peak at 2962 cm⁻¹ in all three samples i.e., the control and treated (T1 and T2). The aromatic C=C stretching of naphthyl moiety was appeared in the region of 1508-

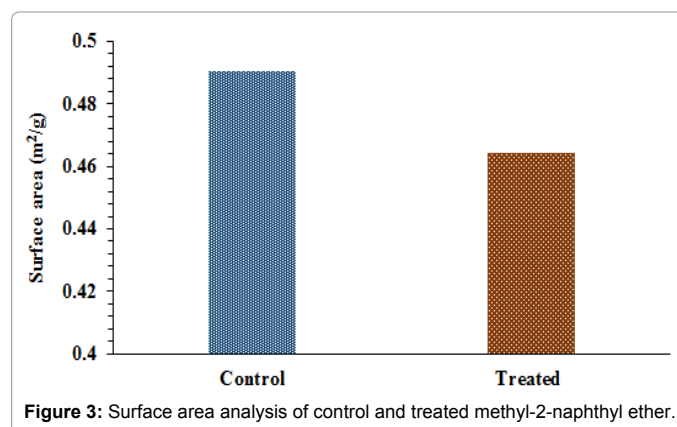


Figure 3: Surface area analysis of control and treated methyl-2-naphthyl ether.

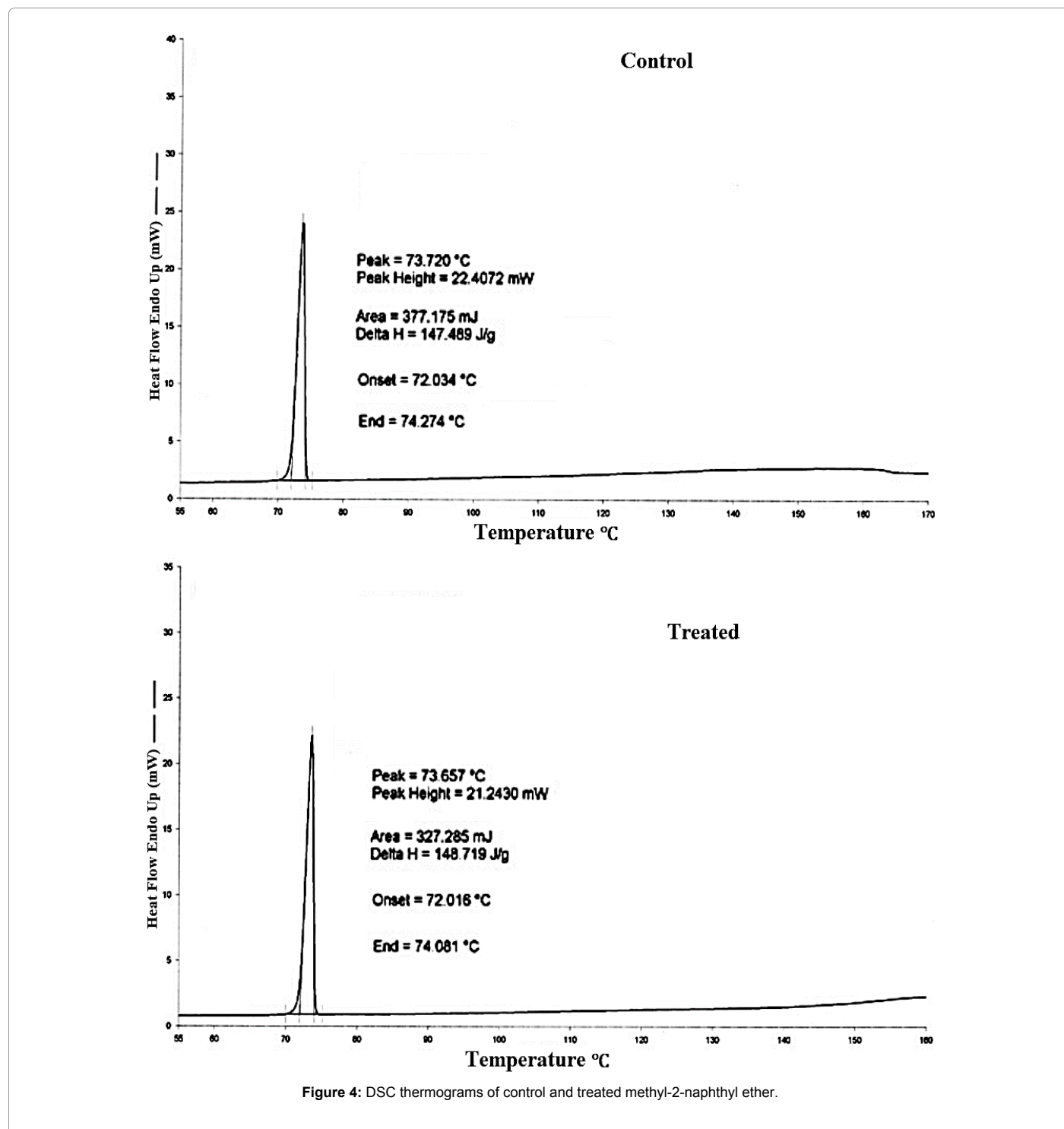


Figure 4: DSC thermograms of control and treated methyl-2-naphthyl ether.

Parameter	Control	Treated
Latent heat of fusion (J/g)	147.49	148.72
Melting point (°C)	73.72	73.66
Onset temperature (°C)	158.00	124.00
End-set temperature (°C)	201.00	178.00
T _{max} (°C)	177.81	153.78

T_{max}: temperature at maximum weight loss occurs

Table 1: Thermal analysis of control and treated samples of methyl-2-naphthylether.

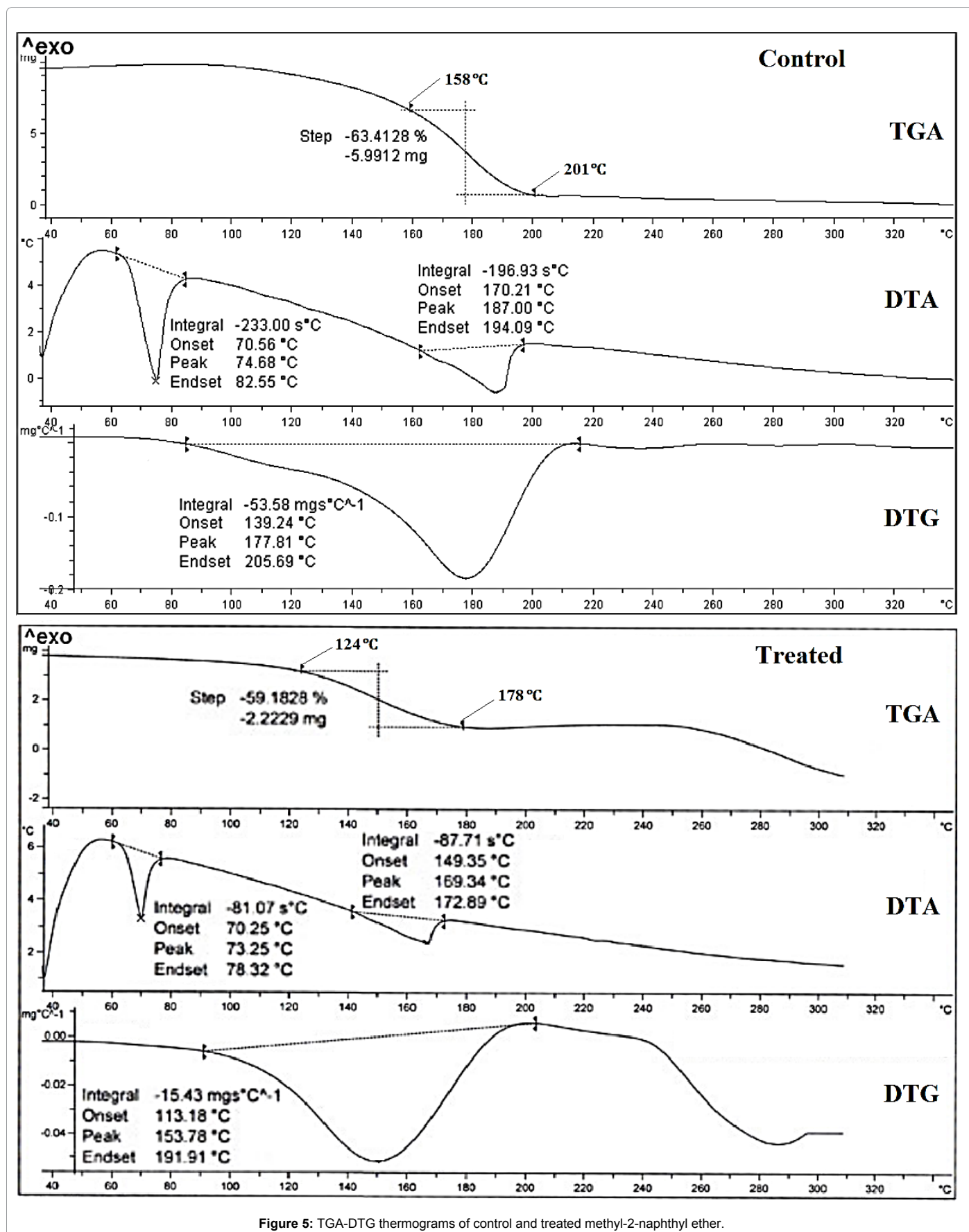


Figure 5: TGA-DTG thermograms of control and treated methyl-2-naphthyl ether.

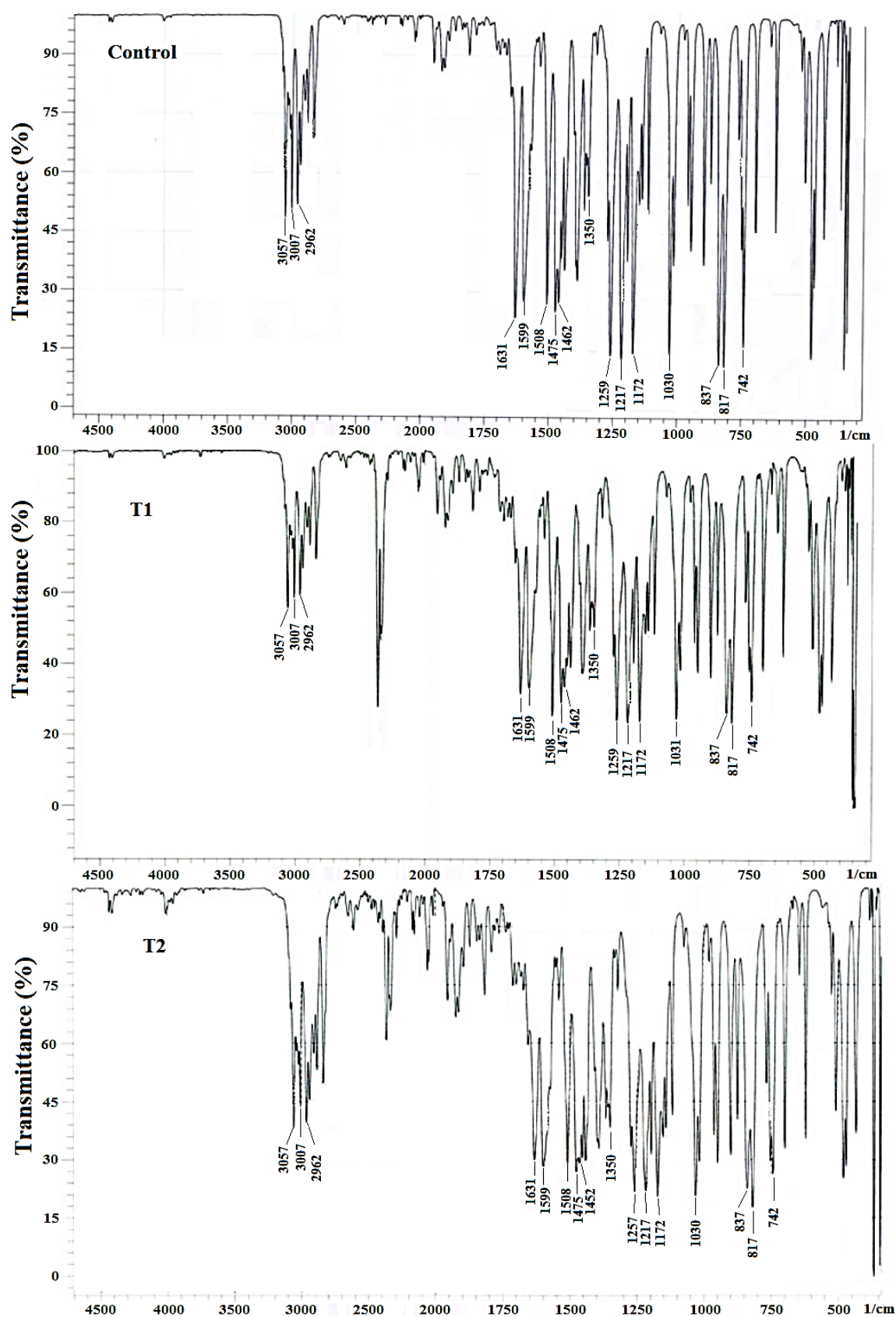


Figure 6: FT-IR spectra of control and treated (T1 and T2) methyl-2-naphthyl ether.

1631 cm^{-1} in all the control and treated samples. The C-H asymmetrical bending peaks were observed at 1462-1475 cm^{-1} in the control and T1 sample; whereas, this peak was observed at 1452-1475 cm^{-1} region in T2 sample. In addition, the C-H symmetrical bending peak was observed at 1350 cm^{-1} in all three samples. The C-O stretching for ether linkage was observed at 1030 cm^{-1} in the control and the T2 sample while 1031 cm^{-1} in the T1 sample. The =C-H in-plane deformation peaks were observed at the frequency region of 1172-1259 cm^{-1} , whereas the C-H out of plane deformation peaks were observed at 742-837 cm^{-1} in all three samples. The observed FT-IR spectra were well supported with the literature data [33].

Uv-Vis spectroscopy

The UV spectra of control and treated (T1 and T2) samples are shown in Figure 7. The UV spectrum of control MNE exhibited the

three different absorption maxima (λ_{max}) at 225.4, 270.4, and 327.2 nm. The UV spectrum of T1 sample showed the similar pattern of λ_{max} i.e., at 224.4, 270.4, and 327.2 nm. Whereas, the T2 sample exhibited the λ_{max} at 233.0, 270.5, and 327.0 nm. The result indicated the shifting of λ_{max} in T2 sample (233.0 nm) as compared to control (225.4 nm). Although, no change in λ_{max} was observed in T1 sample of MNE. Overall, the UV-vis spectral analysis suggests that biofield energy treatment may not cause any significant alterations in the λ_{max} of treated MNE samples with respect to the control.

Conclusion

In brief, the XRD diffractogram of biofield treated MNE exhibited the decrease in intensity of XRD peaks as well as the decrease in average crystallite size (30.70%) as compared to the control. The surface area analysis showed an increase (5.32%) in surface area of biofield treated

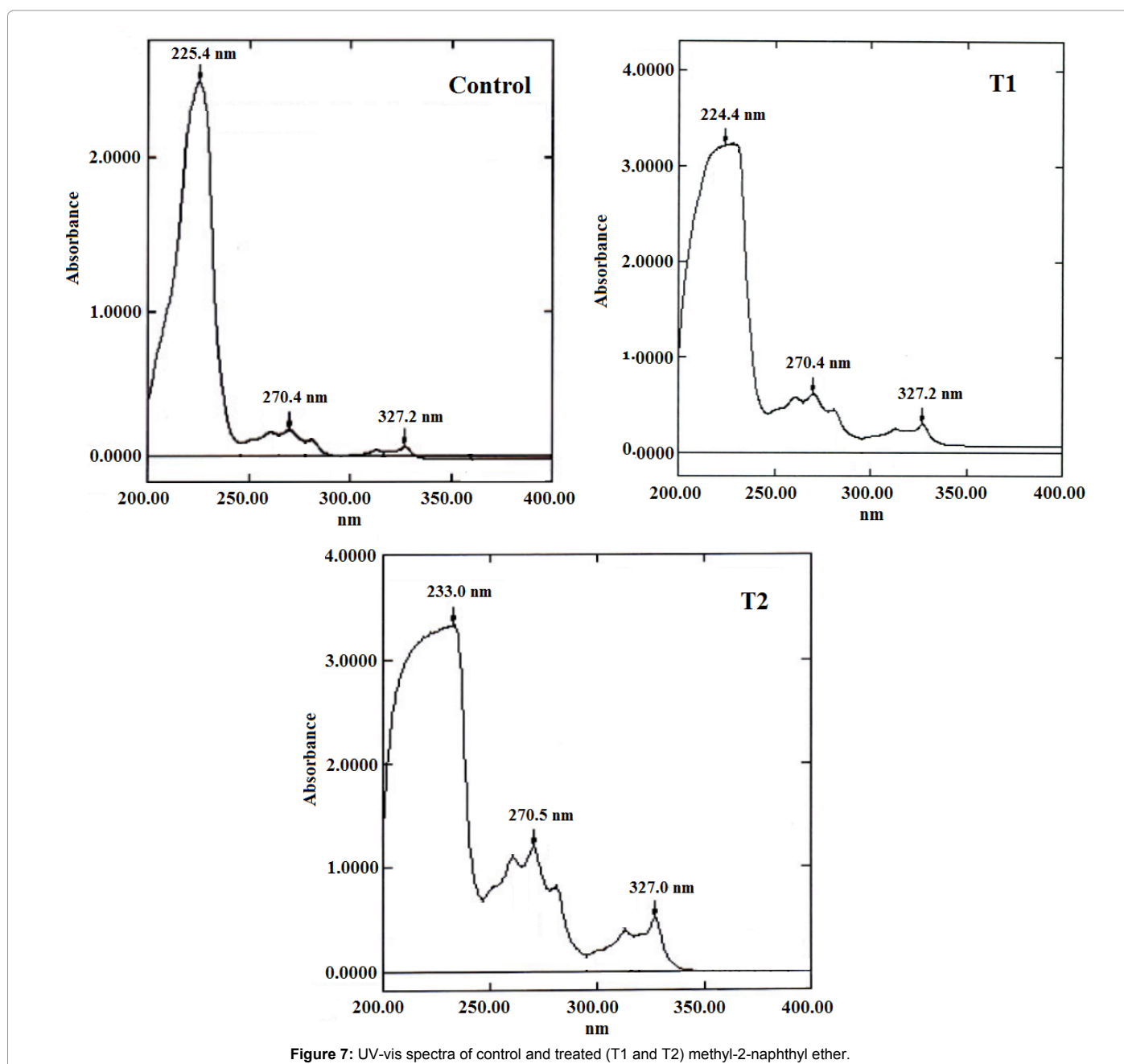


Figure 7: UV-vis spectra of control and treated (T1 and T2) methyl-2-naphthyl ether.

MNE with respect to the control. The thermal analysis (DSC, TGA/DTG) showed a decrease in T_{max} by 13.51%. Moreover, the latent heat of fusion was slightly increased by 0.83% in treated sample as compared to the control.

Overall, it can be concluded that Mr. Trivedi's biofield energy treatment has the impact on physicochemical and thermal properties of treated MNE with respect to the control. Based on this, it is assumed that biofield treated MNE could be more useful chemical intermediate in the organic synthesis of various pharmaceutical drugs.

Acknowledgement

The authors like to acknowledge the Trivedi Science, Trivedi Master Wellness and Trivedi Testimonials for their steady support during the work. Authors would also like to thanks the whole team from the MGV pharmacy college, Nashik for providing the instrumental facility.

References

1. Rokade YB, Sayyed RZ (2009) Naphthalene derivatives: A new range of antimicrobials with high therapeutic value. *Rasayan J Chem* 2: 972-980.
2. Wilson CO, Gisvolds O, Block JH, Beale JM (2004) Textbook of organic medicinal and pharmaceutical chemistry. Lippincott, Williams and Wilkins, Philadelphia.
3. Rokade Y, Dongare N (2010) Synthesis and antimicrobial activity of some azetidinone derivatives with the naphthol. *Rasayan J Chem* 3: 641-645.
4. Pandya AB, Prajapati DG, Pandya SS (2012) Synthesis of novel naphthalene COX inhibitors for anti-inflammatory activity. *J Appl Pharm Sci* 2: 226-232.
5. Cavrini V, Roveri P, Gatti R, Ferruzzi C, Panico AM, et al. (1982) Synthesis of 2-methoxynaphthalene derivatives as potential anti-inflammatory agents. *Farmaco Sci* 37: 171-178.
6. Lednicer D (2007) The organic chemistry of drug synthesis. John Wiley & Sons INC., Hoboken, New Jersey, USA.
7. Koithan M (2009) Introducing Complementary and Alternative Therapies. *J Nurse Pract* 5: 18-20.
8. Hok J, Tishelman C, Ploner A, Forss A, Falkenberg T (2008) Mapping patterns of complementary and alternative medicine use in cancer: an explorative cross-sectional study of individuals with reported positive "exceptional" experiences. *BMC Complement Altern Med* 8: 28.
9. Aldridge D (1991) Spirituality, healing and medicine. *Br J Gen Pract* 41: 425-427.
10. Cahil M (1999) Nurses handbook of complementary and alternative therapies. Springhouse, PA: Springhouse Corporation.
11. Movaffaghi Z, Farsi M (2009) Biofield therapies: biophysical basis and biological regulations complement *Ther Clin Pract* 15: 35-37.
12. Benor DJ (1990) Survey of spiritual healing research. *Complement Med Res* 4: 9-33.
13. Rubik B, Brooks AJ, Schwartz GE (2006) In vitro effect of Reiki treatment on bacterial cultures: Role of experimental context and practitioner well-being. *J Altern Complement Med* 12: 7-13.
14. Rein G (1995) The in vitro effect of bioenergy on the conformational states of human DNA in aqueous solutions. *Acupunct Electrother Res* 20: 173-180.
15. Prakash S, Chowdhury AR, Gupta A (2015) Monitoring the human health by measuring the biofield "aura": An overview. *IJAER* 10: 27637-27641.
16. Trivedi MK, Patil S, Tallapragada RM (2013) Effect of biofield treatment on the physical and thermal characteristics of silicon, tin and lead powders. *J Material Sci Eng* 2: 125.
17. Trivedi MK, Tallapragada RM, Branton A, Trivedi D, Nayak G, et al. (2015) Potential impact of biofield treatment on atomic and physical characteristics of magnesium. *Vitam Miner* 3: 129.
18. Trivedi MK, Nayak G, Patil S, Tallapragada RM, Latiyal O (2015) Evaluation of biofield treatment on physical, atomic and structural characteristics of manganese (II, III) oxide. *J Material Sci Eng* 4: 177.
19. Trivedi MK, Patil S, Shettigar H, Bairwa K, Jana S (2015) Effect of biofield treatment on spectral properties of paracetamol and piroxicam. *Chem Sci J* 6: 98.
20. Trivedi MK, Patil S, Shettigar H, Bairwa K, Jana S (2015) Spectroscopic characterization of biofield treated metronidazole and tinidazole. *Med Chem* 5: 340-344.
21. Sances F, Flora E, Patil S, Spence A, Shinde V (2013) Impact of biofield treatment on ginseng and organic blueberry yield. *Agrivita J Agric Sci* 35: 22-29.
22. Shinde V, Sances F, Patil S, Spence A (2012) Impact of biofield treatment on growth and yield of lettuce and tomato. *Aust J Basic Appl Sci* 6: 100-105.
23. Patil SA, Nayak GB, Barve SS, Tembe RP, Khan RR (2012) Impact of biofield treatment on growth and anatomical characteristics of *Pogostemon cablin* (Benth.). *Biotechnology* 11: 154-162.
24. Trivedi MK, Patil S, Shettigar H, Gangwar M, Jana S (2015) Antimicrobial sensitivity pattern of *Pseudomonas fluorescens* after biofield treatment. *J Infect Dis Ther* 3: 222.
25. Trivedi MK, Patil S, Shettigar H, Mondal SC, Jana S (2015) Evaluation of biofield modality on viral load of Hepatitis B and C viruses. *J Antivir Antiretrovir* 7: 83-88.
26. Patterson AL (1939) The Scherrer formula for X-Ray particle size determination. *Phys Rev* 56: 978-982.
27. Pavia DL, Lampman GM, Kriz GS (2001) Introduction to spectroscopy. (3rd edn), Thomson Learning, Singapore.
28. Paiva-Santos CO, Gouveia H, Las WC, Varela JA (1999) Gauss-Lorentz size-strain broadening and cell parameters analysis of Mn doped SnO₂ prepared by organic route. *Mat Struct* 6: 111-115.
29. Zhang K, Alexandrov IV, Kilmametov AR, Valiev RZ, Lu K (1997) The crystallite-size dependence of structural parameters in pure ultrafine-grained copper. *J Phys D Appl Phys* 30: 3008-3015.
30. Shih WY, Liu J, Shih WH, Aksay IA (1991) Aggregation of colloidal particles with a finite interparticle attraction energy. *J Stat Phys* 62: 961-984.
31. Armarego WLF, Chai CLL (2013) Purification of laboratory chemicals. (7th edn), Butterworth-Heinemann, Oxford, UK.
32. Pardo G, Moral R, Aguilera E, Del Prado A (2015) Gaseous emissions from management of solid waste: a systematic review. *Glob Chang Biol* 21: 1313-1327.
33. Fazal Mohamed MI, Arunadevi S, Koperuncholan M, Mubarak MS. (2011) Synthesis and antimicrobial activity of some naphthyl ether derivatives. *Der Chemica Sinica* 2: 52-57.